Long-Term Two-Photon Calcium Imaging of Neuronal Populations with Subcellular Resolution in Adult Non-human Primates

AUTHOR(S):

Sadakane, Osamu; Masamizu, Yoshito; Watakabe, Akiya; Terada, Shin Ichiro; Ohtsuka, Masanari; Takaji, Masafumi; Mizukami, Hiroaki; ... Kawasaki, Hiroshi; Matsuzaki, Masanori; Yamamori, Tetsuo

CITATION:

Sadakane, Osamu ...[et al]. Long-Term Two-Photon Calcium Imaging of Neuronal Populations with Subcellular Resolution in Adult Non-human Primates. Cell Reports 2015, 13(9): -1989: 1999.

ISSUE DATE:

2015-12-01

URL:

http://hdl.handle.net/2433/216326

Resource

Cell Reports

Long-Term Two-Photon Calcium Imaging of Neuronal Populations with Subcellular Resolution in Adult Non-human Primates

Graphical Abstract

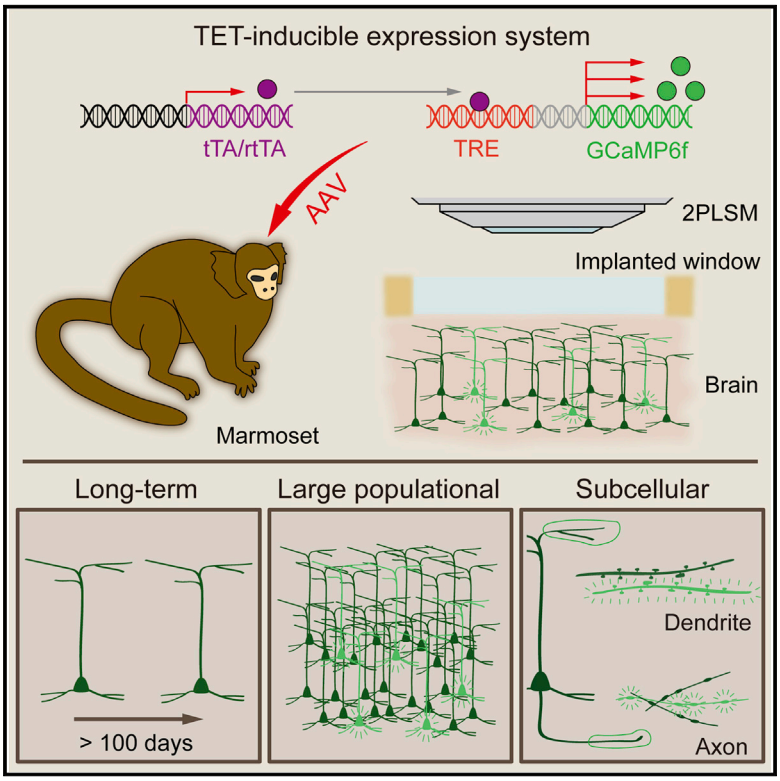

Highlights

- An AAV vector system for enhanced and controllable expression of GCaMP6f is developed
- This system allows long-term two-photon neuronal imaging in the marmoset brain
- The same neuronal populations can be followed over 100 days
- Neuronal responses to tactile stimulation can be imaged at subcellular resolution

Authors

Osamu Sadakane, Yoshito Masamizu, Akiya Watakabe, ..., Hiroshi Kawasaki, Masanori Matsuzaki, Tetsuo Yamamori

Correspondence

mzakim@nibb.ac.jp (M.M.), tetsuo.yamamori@riken.jp (T.Y.)

In Brief

Long-term two-photon calcium imaging has been challenging in non-human primates. Sadakane et al. use an inducible expression system to visualize cortical neurons in adult marmosets. They show that the same neuronal population can be followed over 100 days and neuronal responses to tactile stimulation can be imaged at subcellular resolution.

Sadakane et al., 2015, Cell Reports *13*, 1989–1999
December 1, 2015
http://dx.doi.org/10.1016/j.celrep.2015.10.050

CellPress

Cell Reports
Resource

Long-Term Two-Photon Calcium Imaging of Neuronal Populations with Subcellular Resolution in Adult Non-human Primates

Osamu Sadakane,[1,2,3,8] Yoshito Masamizu,[2,4,8] Akiya Watakabe,[1,2,3,8] Shin-Ichiro Terada,[4,5,8] Masanari Ohtsuka,[1,3] Masafumi Takaji,[1,3] Hiroaki Mizukami,[6] Keiya Ozawa,[6,9] Hiroshi Kawasaki,[7] Masanori Matsuzaki,[2,4,*] and Tetsuo Yamamori[1,2,3,*]

[1]Division of Brain Biology, National Institute for Basic Biology, Aichi 444-8585, Japan
[2]Department of Basic Biology, The Graduate University for Advanced Studies (Sokendai), Aichi 444-8585, Japan
[3]Laboratory for Molecular Analysis of Higher Brain Function, RIKEN Brain Science Institute, Saitama 351-0198, Japan
[4]Division of Brain Circuits, National Institute for Basic Biology, Aichi 444-8585, Japan
[5]Laboratory of Cell Recognition and Pattern Formation, Graduate School of Biostudies, Kyoto University, Kyoto 606-8501, Japan
[6]Division of Genetic Therapeutics, Center for Molecular Medicine, Jichi Medical University, Tochigi 329-0498, Japan
[7]Department of Medical Neuroscience, Graduate School of Medicine, Kanazawa University, Ishikawa 920-8640, Japan
[8]Co-first author
[9]Present address: IMSUT Hospital, The Institute of Medical Science, The University of Tokyo, Tokyo 108-8639, Japan
*Correspondence: mzakim@nibb.ac.jp (M.M.), tetsuo.yamamori@riken.jp (T.Y.)
http://dx.doi.org/10.1016/j.celrep.2015.10.050

SUMMARY

Two-photon imaging with genetically encoded calcium indicators (GECIs) enables long-term observation of neuronal activity in vivo. However, there are very few studies of GECIs in primates. Here, we report a method for long-term imaging of a GECI, GCaMP6f, expressed from adeno-associated virus vectors in cortical neurons of the adult common marmoset (*Callithrix jacchus*), a small New World primate. We used a tetracycline-inducible expression system to robustly amplify neuronal GCaMP6f expression and up- and downregulate it for more than 100 days. We succeeded in monitoring spontaneous activity not only from hundreds of neurons three-dimensionally distributed in layers 2 and 3 but also from single dendrites and axons in layer 1. Furthermore, we detected selective activities from somata, dendrites, and axons in the somatosensory cortex responding to specific tactile stimuli. Our results provide a way to investigate the organization and plasticity of cortical microcircuits at subcellular resolution in non-human primates.

INTRODUCTION

Two-photon imaging using genetically encoded calcium indicators (GECIs) has been applied to a variety of invertebrates and vertebrates including flies, fish, and rodents and has provided deep insight into the neural circuits in live animals. For example, studies on mice have revealed the organization of neocortical neurons at single-cell resolution in the sensory cortex (Andermann et al., 2011; O'Connor et al., 2010). Others have studied the reorganization of cortical circuits during behavioral training in sensorimotor (Huber et al., 2012; Masamizu et al., 2014; Peters et al., 2014) and cognitive tasks (Chen et al., 2013a; Harvey et al., 2012). Two-photon imaging with GECIs can also be applied to detect neuronal activities in fine structures such as dendrites and axons. For example, in the mouse visual cortex, stimulus-tuned inputs to dendrites were observed to persist stably for weeks (Chen et al., 2013b). Other studies have clarified the stimulus selectivity of cortical axonal outputs to adjacent areas (Glickfeld et al., 2013; Matsui and Ohki, 2013; Petreanu et al., 2012). Thus, applications of GECIs to mice have had a large impact on investigations of the organization and plasticity of neuronal circuits.

In contrast to the mouse studies, studies on functional imaging with GECIs using non-human primates are very scarce. In one pioneering study of a GECI applied to macaques, the activities of visual cortical neurons were imaged for months through a chronically implanted window (Heider et al., 2010). However, only several neurons were simultaneously imaged in the same field and the same neurons were not followed over the imaging period. Although synthetic calcium indicator dyes have been successfully used in two-photon imaging to detect the highly organized structures of the primary visual cortex of macaque monkeys (Ikezoe et al., 2013; Nauhaus et al., 2012), they cannot be used for long-term recording of population activity or imaging of subcellular activity. Considering the importance of primate studies in understanding higher cognitive abilities of the human cerebral cortex, one should challenge the improvement of GECI technology so that it can be applied to non-human primates. Among non-human primates, the common marmoset has a much-smaller brain than the macaque. Nonetheless, it exhibits essential

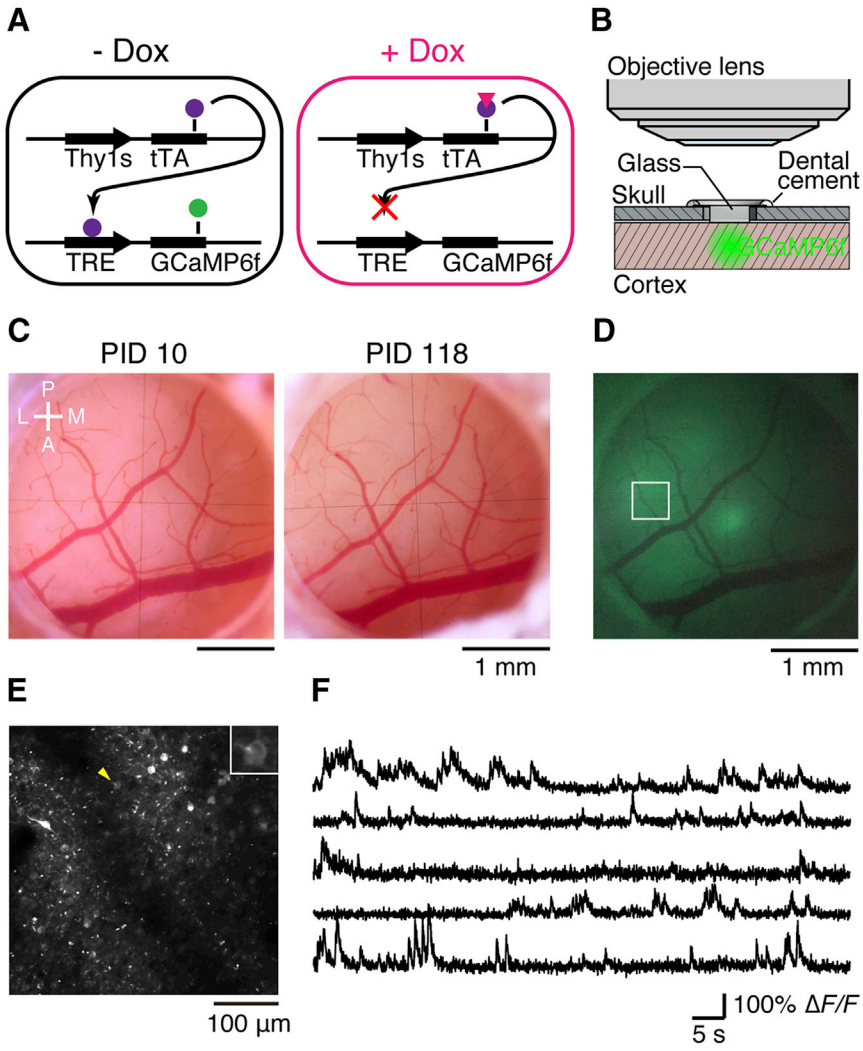

Figure 1. In Vivo Two-Photon Calcium Imaging in the Marmoset Neocortex Using the TET-Off System

(A) Schematic illustration of the TET-Off gene expression system. tTA (purple circles) activates the TRE3 promoter to amplify GCaMP6f (green circle) expression. Dox (pink triangle) inhibits the binding of tTA to the TRE3 promoter.

(B) Schematic illustration of the imaging window. "Glass" indicates four sheets of 3-mm circular glass coverslips that were adhered to a 5.5-mm circular glass coverslip.

(C) Vasculature images from the same imaging window obtained on postinjection day (PID) 10 and PID 118. A, anterior; L, lateral; M, medial; P, posterior.

(D) Epifluorescence image from the same window as shown in (C) on PID 10. The rectangle indicates the field shown in (E).

(E) Two-photon image of GCaMP6f in the rectangle shown in (D). The image was averaged across 4,500 continuous frames. The depth of the image was 250 μm from the cortical surface. The inset is an enlarged view of a single cell (yellow arrowhead).

(F) Representative $\Delta F/F$ traces from five ROIs in the field shown in (E). The top trace is from the cell shown in the enlarged view in (E).

See also Figures S1 and S2.

features of primate cortical organization (Krubitzer and Kaas, 1990; Roberts et al., 2007). Considering that two-photon imaging of the mouse brain can image the morphology of the neuronal somata up to a depth of 1.4 mm from the cortical surface (Kawakami et al., 2013) and neuronal activity up to a depth of 0.6 mm (Glickfeld et al., 2013; Masamizu et al., 2014), the relatively thin (approximately 1.5- to 2-mm thickness) and smooth cerebral cortex of marmosets should have a big advantage over cerebral cortex of larger primates when it comes to three-dimensionally detecting cortical neuronal activity by two-photon imaging.

Here, we developed an adeno-associated virus (AAV)-based system for long-term calcium imaging of adult common marmosets. To amplify the transgene expression from AAV vectors, we adapted the tetracycline-inducible gene expression system (TET-inducible system) that we have been using to amplify transgene expression from lentiviral vectors (Hioki et al., 2009; Watakabe et al., 2012). We found that the signal amplification in the TET-inducible system in the marmoset was so effective that GCaMP6f signals could be detected only 10 days postinjection. The expression level of GCaMP6f was controllable by doxycycline (Dox) administration in both TET-Off and TET-On systems, which shut off and turn on the expression by Dox, respectively (Lewandoski, 2001). As a result, the integrity of transduced cortical neurons could be maintained for weeks and months. We were able to monitor spontaneous activity and sensory responses from somata, dendrites, and axons of individual cortical neurons in anesthetized adult marmosets.

RESULTS

Two-Photon Calcium Imaging of the Marmoset Brain with a TET-Inducible System

To construct a TET-inducible system for AAV (AAV TET-inducible system), we first cloned two components of the TET-Off system, namely, the tetracycline-controlled transactivator (tTA) under the control of the Thy1S promoter (Ako et al., 2011; a modified version of Thy1 promoter, described in Experimental Procedures in detail) and GCaMP6f under the control of the tetracycline response element (TRE3) promoter, into separate AAV vectors (Figure 1A). In the absence of Dox, tTA constitutively activates expression of a transgene under the TRE3 promoter. Dox prevents the binding of the tTA to the TRE3 and inhibits transgene expression (Figure 1A).

For AAV injection into the marmoset neocortex, a hole (~4 mm in diameter) was created in the skull. The exposed dura mater

was removed because it became opaque after exposure, unlike the dura mater of mouse brains (Stettler et al., 2006). Then, AAVs carrying Thy1S-tTA and TRE3-GCaMP6f were injected together into the cerebral cortices of two adult marmosets: into the parietal cortex of one animal and the somatosensory cortex of another. The imaging window should remain transparent for a long time to allow good two-photon imaging in vivo. In addition, it should be stably attached to the cortical surface to reduce motion artifacts induced by pulsation and breathing even under anesthesia. To tightly fill the space between the top skull surface and the cortical surface with the imaging window, we devised an assembly that consists of cover glasses that are bonded together with optical adhesives (Figures 1B and 1C; see Experimental Procedures for more details). Immediately after the AAV injection, the glass assembly was inserted into the hole and gently pushed on the cortical tissue to reduce brain motion during imaging. The blood vessel patterns were clearly observed through the imaging window immediately after the surgery and did not substantially change for more than 4 months (Figure 1C). This indicates that the imaging window did not cause any apparent damage to the cortical surface.

For fluorescence imaging after AAV injection, marmosets were placed under the microscope and lightly anesthetized by isoflurane inhalation. The plane of the imaging window was adjusted to be nearly perpendicular to the optical axis by changing the angle of tilt of the marmoset chair stage (~5–10 degrees). As expected from the high-level transgene expression obtainable with the TET-inducible system (Hioki et al., 2009), we detected strong epifluorescence signals around the injection site through the imaging window after only 10 days of AAV injection (Figure 1D). When we performed two-photon imaging near the injection site at an excitation wavelength of 940 nm (Chen et al., 2013b), bright signals of GCaMP6f were observed from individual cell bodies in layer 2 (L2), located at depths of >90 μm from the cortical surface (Hardman and Ashwell, 2012; Figure 1E). After motion correction (Thévenaz et al., 1998), a region of interest (ROI) was determined for each fluorescently detected neuronal soma. The relative change in fluorescence ($\Delta F/F$) in each ROI did not exhibit fast up and down deflections (Figure 1F), indicating that the imaging window effectively reduced the motion artifact along the optical axis that cannot be digitally corrected. In many neurons, spontaneous calcium transients were clearly detected (Figure 1F), as reported for other animals (Chen et al., 2013b). The $\Delta F/F$ trace in each ROI did not show any photobleaching for at least 10 min.

The effectiveness of the AAV "TET-Off" vectors was obvious when we compared this result with the conventional AAV2/1 encoding GCaMP6f under the control of the Synapsin I promoter. Even 2 months after injection, the fluorescence signals of GCaMP6f from the conventional AAV were too weak to be detected in vivo. In the fixed cortical tissue, GCaMP6f signals were immunohistochemically detected in many neurons, albeit at a low level (Figure S1). Interestingly, injection of the same batch of Synapsin I-GCaMP6f AAV into the mouse neocortex led to bright fluorescence of GCaMP6f during two-photon imaging in vivo (Chen et al., 2013b). We concluded that the marmoset brain requires high amplification of the GCaMP6f signals (e.g., by the TET-Off system) for successful in vivo two-photon calcium imaging.

In addition to the TET-Off system, we also tested a TET-On system to see whether we could induce GCaMP6f expression by Dox administration to the marmoset. For this purpose, we injected AAVs carrying Synapsin I-rtTA (Watakabe et al., 2014; Figure S2A) and TRE3-GCaMP6f into the somatosensory cortex and performed in vivo imaging. Without Dox administration, epifluorescence was not detected (Figure S2B) after 3 weeks of AAV injection. However, after only 3 days of Dox administration, epifluorescence was clearly detected around the injection sites and GCaMP6f signals were detected from many neurons at higher magnification (Figures S2C–S2E). The induced epifluorescence returned to the baseline level 2 to 3 weeks after the removal of Dox (Figures S2F and S2G). Thus, both TET-Off and TET-On systems can be used for two-photon imaging of the adult marmoset and the system best suited to the experimental design can be selected.

Long-Term Two-Photon Calcium Imaging of Multiple Neurons

Having succeeded with the initial imaging, we went on to test whether long-term imaging experiments were possible. It has been reported that transgene expression from AAV gradually increases over a period of up to 2 months (Diester et al., 2011), and this could result in toxicity in experiments that last for several weeks or months (Chen et al., 2013b; Tian et al., 2009). In this regard, the AAV TET-inducible system offers the advantage of controlling transgene expression by Dox administration. To test the effectiveness of Dox control in marmosets injected with AAV-TET-Off vectors, we administered Dox in drinking water to the animals for several days and examined an image of the same area repeatedly over time. The imaging fields in the two marmosets with the AAV-TET-Off vectors as well as the schedules of the imaging and Dox administration are shown in Figure S3. In a representative experiment in marmoset A, 5 days of Dox administration resulted in a gradual decrease of fluorescence signals, and this decrease lasted even after Dox administration was stopped (Figure 2A). The fluorescence signals did not start to increase until approximately 10 days after Dox had been removed from the drinking water and then gradually increased to the original level by approximately 20–30 days after the termination of Dox administration (Figures 2A and 2B). A similar time course was observed in the imaged fields from marmoset B (Figure 2B).

Importantly, 28 days after the start of the 5-day Dox administration, we were able to identify the same population of neurons that we observed before Dox administration (Figure 2A). Spontaneous calcium transients were detected from the same neuron both before and after Dox administration (Figure 2C). In marmoset B, after a 1-month recovery from 7-day Dox administration, the activity of many neuronal somata were clearly detected within a relatively broad field of 625 × 625 μm in L2 (Figures 2D and 2E). The half-decay time of calcium transients was 0.311 ± 0.040 s (mean ± SEM; n = 28 from Figure 2D; Figures 2F and 2G), which was comparable with that of the original report for GCaMP6f (Chen et al., 2013b). We observed a set of neurons with very similar configurations at an interval of more than 100 days after three trials of Dox administration, which are most likely to represent identical neuronal populations (Figure S4).

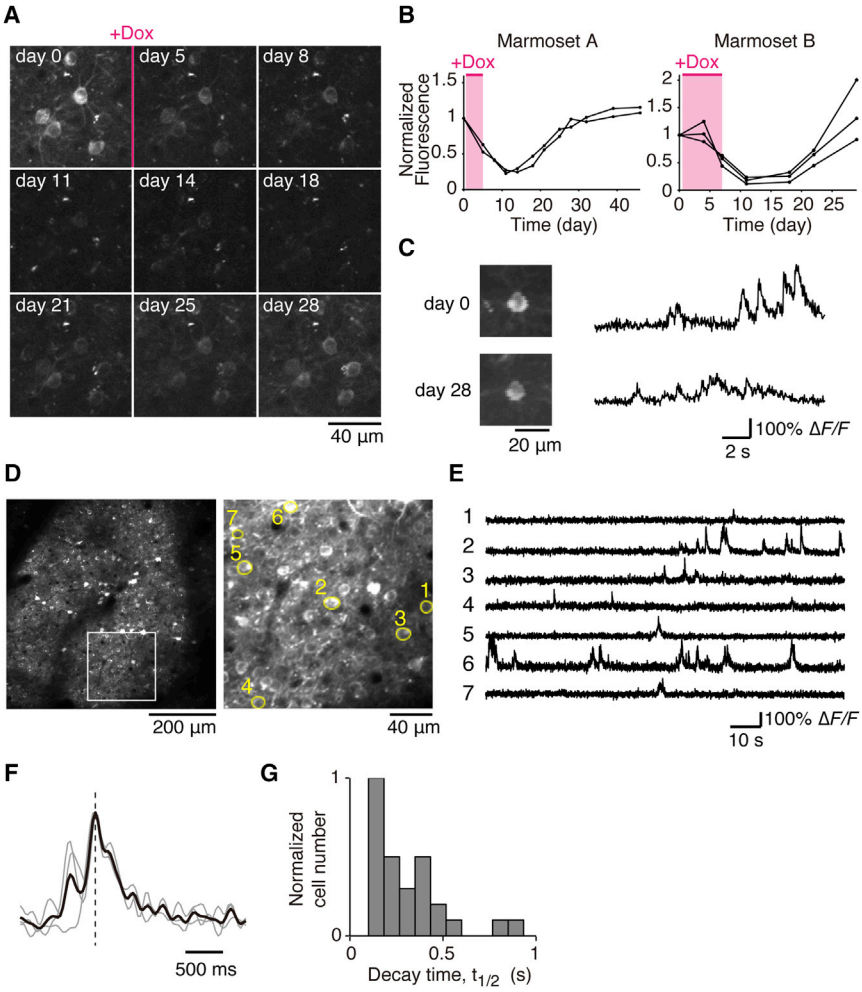

Figure 2. Expression Control of GCaMP6f by Dox Administration

(A) Representative two-photon images that show the effects of Dox administration on the expression level of GCaMP6f. The same region of the parietal cortex in marmoset A was chronically imaged before and after Dox administration. The day of onset of Dox administration is set at day 0. The image on day 0 was acquired before Dox administration started. The depth of the image was 140 μm.

(B) Time course of the averaged fluorescence intensity within the field on each imaging day before, during, and after the Dox administration (red shading). The fluorescence intensity was normalized to that on day 0. In marmoset A, Dox was administered for 5 days and two fields were measured. In marmoset B, Dox was administered for 7 days and three fields were measured.

(C) Images of and representative Δ*F*/*F* traces from the same neuron immediately before (top) and 28 days after (bottom) Dox administration started.

(D) Representative two-photon images of GCaMP6f 32 days after Dox administration started. The depth of the image is 150 μm. The white rectangle field in the left panel is expanded in the right panel.

(E) Representative Δ*F*/*F* traces from the seven ROIs indicated by yellow circles in (D).

(F) Three traces (gray) and the average trace (black) of calcium transients in the second ROI in (E), aligned to the timing of the peak. Amplitude is normalized to peak amplitude.

(G) Histogram of half-decay time (n = 28).

See also Figures S3, S4, and S5.

To test the integrity of the tissue around the injection site after long-term imaging, we sacrificed marmoset A for immunohistochemical examination more than 100 days after AAV injection. Figure 3A shows the native fluorescence of GCaMP6f (green) counterstained with NeuN (red). Except for a small needle scar at the center of the injection site (shown by an asterisk), we observed no sign of tissue damage despite strong GCaMP6f expression. In this particular injection site, AAV had spread approximately 700–1,000 μm horizontally and covered the depth of layer 1 (L1) through to layer 5 (Figure 3A). At higher magnification, we saw relatively few pyramidal cells with strong positive GCaMP6f expression and numerous neurons with moderate-to-low GCaMP6f expression (Figure 3B), which is consistent with the in vivo imaging data.

The fluorescently labeled neurons included parvalbumin-positive neurons in addition to pyramidal neurons (Figures 3C and 3D). These results indicate that appropriate Dox administration can achieve sufficiently high expression of GCaMP6f in many excitatory and inhibitory neurons at imaging time points over more than 100 days and can prevent the cell damage that is associated with extremely high transgene expression.

One characteristic feature of the marmoset brain that we observed was the presence of granule-like fluorescent structures in the imaging regions (e.g., Figures 2A, 2D, S2D, and S4). Most of them had strong fluorescence in both red and green channels, and they were detected not only at the AAV injection site but also in the contralateral side (non-injection site) in cortical slices (Figure S5). Based on the spectral features and prevalent distribution in both injected and non-injected regions, we considered these granule-like fluorescent structures to be tissue autofluorescent (most likely lipofuscin; Eichhoff et al., 2008; Honavar and Lantos, 1987; Mochizuki et al., 1995) and not the aggregation of overexpressed GCaMP6f. In addition, we observed bright green spots with no fluorescence in the red channel in in vivo imaging (Figure S4). These spots were detected at similar horizontal locations over a depth of >20 μm, and we therefore considered these to be the cross-section of apical dendrites of neurons with expression of GCaMP6f. Although we cannot exclude the possibility that a minor subset of granule-like fluorescent structures came from the accumulation of GCaMP6f, here we note the existence of granular tissue autofluorescence as a characteristic feature of the adult marmoset brain, of which origin should be identified in the future.

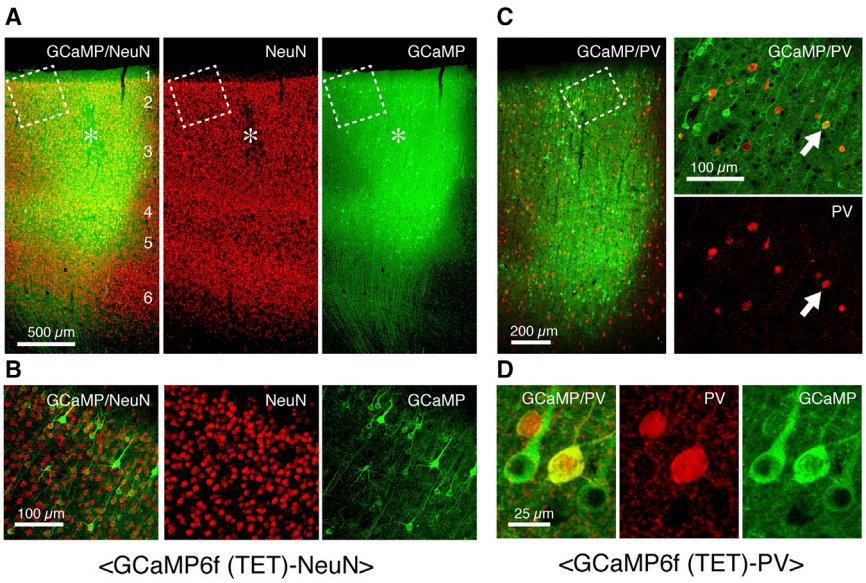

Figure 3. Histological Identification of GCaMP6f-Transduced Neurons

(A) A sample injected with AAV-TET-Off vectors and immunostained with the antibody to NeuN.

(B) High-power views of the dotted rectangle in (A).

(C) A sample injected with AAV-TET-Off vectors and immunostained with the antibody to parvalbumin (PV). The right panel is the high-power views of the dotted rectangle in the left panel. The arrows in the right panel indicate examples of PV-positive interneurons expressing GCaMP6f.

(D) The magnified views around the arrows in the right panel of (C).

(A)–(D) are representative images from a total of three different slices.

Two-Photon Calcium Imaging of Individual Dendrites and Axons

Next, we determined whether neuronal activity in subcellular compartments that include dendrites and axons can be detected using AAV-TET-Off vectors. To image the subcellular activity, we decreased the size of the scanning field in L1 and digitally increased the pixel size. We could clearly detect some dendrites with spontaneous calcium transients with a high signal-to-noise ratio (Figures 4A and 4B). In many cases, calcium transients occurred throughout single dendritic branches (e.g., Figures 4A and 4B; d1), including dendritic spines (e.g., Figures 4A and 4B; s1), indicating that the calcium transients reflected backpropagation of action potentials and/or dendritic spiking (Chen et al., 2013b; Xu et al., 2012). We also detected some axonal boutons with synchronous calcium transients within a scanning field (Figures 4C and 4D; ROI 3–7), indicating that these boutons originated from the same axon and that the calcium transients reflected action potentials (Glickfeld et al., 2013; Petreanu et al., 2012). Thus, the AAV TET-inducible system successfully performed two-photon imaging of the neuronal activity of individual dendrites and axons in the adult marmoset brain.

Three-Dimensional Two-Photon Calcium Imaging of Multiple Neurons

Due to a high signal-to-noise ratio of the fluorescence signals, we were able to monitor the activity of neuronal somata located up to 400 μm from the cortical surface. This depth range is supposed to cover L1 and L2, as well as the upper part of layer 3 (L3) (Figure 3A). Using a piezoelectric objective mount, we continuously recorded the activity of multiple neurons with single-cell resolution from a relatively broad area (625 × 625 μm) at three depths: 150 μm; 275 μm; and 400 μm (from L2 to L3; Figure 5A). The frame rate was 4.17 Hz for each plane. In this experiment, 445 putative neuronal somata were determined and 81 of them were spontaneously active neurons (18/146, 29/168, and 34/131 with a skewness of $\Delta F/F > 0.5$ at a depth of 150 μm, 275 μm, and 400 μm, respectively; Figures 5B and 5C). These data can be used to analyze the spatial and functional relations between large numbers of neurons dispersed in three dimensions. For example, for pairs of active neurons located at the same depth, the pairwise correlation in the time series of $\Delta F/F$ was negatively associated with the cellular distance between the two neurons (Pearson's correlation coefficient = −0.14; $p < 2.88 \times 10^{-5}$; Spearman's rank correlation coefficient test; n = 1,120 pairs; Figure 5D). This is consistent with a previous report in the mouse visual cortex (Hofer et al., 2011). We also found this relation between active neuron pairs located at different depths (Pearson's correlation coefficient = −0.13; $p < 4.25 \times 10^{-7}$; Spearman's rank correlation coefficient test; n = 1,508 pairs; Figure 5E). These examples underscore the effectiveness of our method for investigating the three-dimensional organization of the marmoset cortical microcircuits.

Robust Sensory Selectivity of Neuronal Somata, Dendrites, and Axons

One strength of calcium imaging is its ability to investigate the spatial and temporal profiles of populations of neurons responding to various types of sensory stimuli. To demonstrate the feasibility of such an approach using our system, we tested whether neuronal responses evoked by tactile stimulation could be detected in the somatosensory cortex. For tactile stimulation, we attached vibrators to the arm and leg of marmoset B that were contralateral to the hemisphere with the imaging window and stimulated each body part alternately for 1 s with an interval of 7.5 s. We found some neurons that responded to the tactile stimulation. Figure 6A shows two examples of neuronal soma in L3, whose fluorescence changes were clearly time locked to the stimuli. Interestingly, responses of these two cells were highly selective to either arm or leg stimuli despite their spatial proximity to each other (Figure 6A). The response was robust in every trial for both neurons. The calcium transient occurred immediately after the onset of the stimulus and declined immediately at the end of the stimulus.

Consistent with the existence of stimulus-selective neurons, we also observed stimulus-selective responses from dendrites in L1 (Figure 6B; Movie S1) and axonal boutons in L1 (Figure 6C).

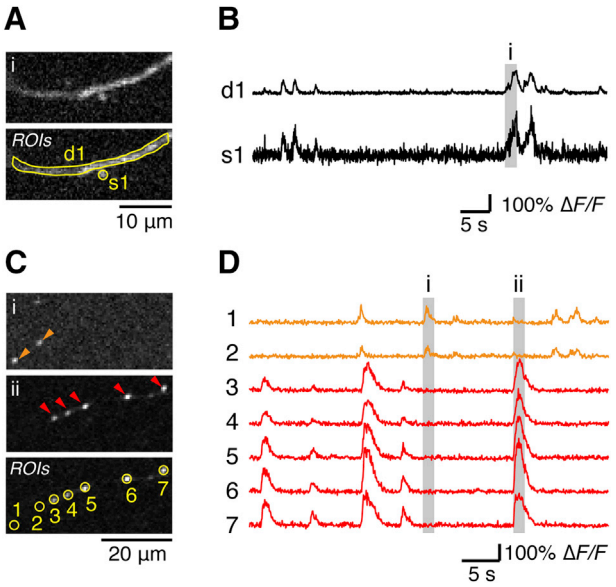

Figure 4. Two-Photon Imaging of GCaMP6f in a Single Dendrite and Two Putative Axons in L1

(A) Images of a dendritic region showing spontaneous calcium transients. The depth of the images is 30 μm from the cortical surface. (Top) Δ*F*/*F* images averaged across 30 continuous frames (denoted by a gray box i in B) with a calcium transient are shown. (Bottom) ROIs of the dendritic shaft (d1) and dendritic spine (s1) are shown.

(B) Representative Δ*F*/*F* traces of the dendritic shaft and spine surrounded by yellow contours in (A). The calcium transients were synchronous in d1 and s1 (i).

(C) Images of axonal boutons showing spontaneous calcium transients. The depth of the images is 20 μm from the cortical surface. (Top and middle) Δ*F*/*F* images averaged across ten continuous frames (denoted by gray boxes i and ii in D) with a calcium transient are shown. Orange and red arrowheads indicate putative axonal boutons. (Bottom) ROIs of the axonal boutons are shown.

(D) Representative Δ*F*/*F* traces of seven axonal ROIs indicated by yellow contours in (C). Note that the same color ROIs showed synchronous calcium transients, but the timing of the calcium transients was different between orange and red ROIs (i and ii).

The responses of these dendrites and axons to each stimulus were as robust as those of the somata. Thus, our results demonstrate that the spatial and temporal profile of each neuron, dendrite, and axon in the marmoset cerebral cortex can be correlated with a variety of sensory stimuli.

DISCUSSION

In this study, we demonstrated the quality of two-photon calcium imaging with GCaMP6f in non-human primate brains. The key to our technique was the adaptation of an AAV TET-inducible system that enabled high amplification of the GCaMP6f signal as well as control of this signal by Dox administration. We also improved the assembly setup of the imaging window so that it retains clear and stable paths for two-photon imaging that can last for months. We showed that it is possible to (1) simultaneously record hundreds of neurons, (2) repeatedly image the same neuronal populations over weeks and months, and (3) reliably detect calcium transients in dendrites and axonal boutons.

Transgene control by the TET-inducible system has previously been effectively used to fixate memory engrams in mice (Liu et al., 2012) and for pathway-specific blockage of neurotransmission in mice and macaques (Kinoshita et al., 2012; Sooksawate et al., 2013). We proved the usefulness of this system for calcium imaging in marmosets. Our system could also be useful in mice to prevent the adverse effect of GECI overexpression (Chen et al., 2013b; Tian et al., 2009), although we have yet to establish the optimal protocol for Dox control to reduce the time lag between Dox manipulation and transgene up- and downregulation (Figure 2). To enhance the utility of the current method, it is also important to develop cell-type-specific labeling for non-mouse species. For example, two-point viral injection approaches, in which retrograde and anterograde viral vectors are injected into the target and origin of projection, are a promising method for labeling specific cortical projection neurons such as corticospinal, corticocortical, and corticothalamic neurons (Masamizu et al., 2011, 2014; Watakabe et al., 2014). The AAV TET-inducible system would also be useful for achieving sufficiently high expression of Channelrhodopsin-2 to induce hand and/or arm behaviors in the primate, which have not yet been reported (Gerits and Vanduffel, 2013). Generally speaking, the purity of the virus vector can affect infectivity, especially in cases where a large amount is used. In this regard, amplification by the TET-inducible system has merit in that it allows us to induce robust transgene expression at a relatively low titer.

Two-photon imaging with GECIs is a powerful tool to compensate for a variety of electrical recording methods. Whereas two-photon imaging lacks the high temporal resolution of electrical recording (>10 ms versus <1 ms for electrical recording), it can record many neurons with precisely identified locations. With the current technique, we were able to record the activities of 445 neurons distributed in three different planes of marmoset L2 and L3. Furthermore, a recent development now allows simultaneous observation of distant locations by two-photon imaging (Lecoq et al., 2014), which partly compensates for the limited area of coverage provided by subdural grid electrodes (Khodagholy et al., 2015). One big advantage of two-photon imaging is that it is possible to resolve images at the level of the individual dendrite and axon. Thus, the two-photon calcium-imaging technique that we have developed in this report should greatly expand our ability to investigate non-human primate brains beyond what can be achieved by relying on electric recording techniques. This should especially be the case for the study of long-term cortical reorganization.

Plasticity of the cortical circuit is an important feature of the primate brain, although it is not unique to primates. For example, there are somatosensory map changes following digit or limb amputation in adult macaques and humans (Flor et al., 1995; Merzenich et al., 1984). Injury to the primary motor cortex of the macaque also leads to extensive reorganization involving premotor areas over a period of 5 months (Dancause et al., 2005). Visuomotor learning also reorganizes the neuronal activity in the macaque premotor cortex (Mitz et al., 1991). Long-term calcium imaging of the structure and function of axons and dendritic spines should be useful to investigate the mechanisms by which such cortical reorganization occurs in primates.

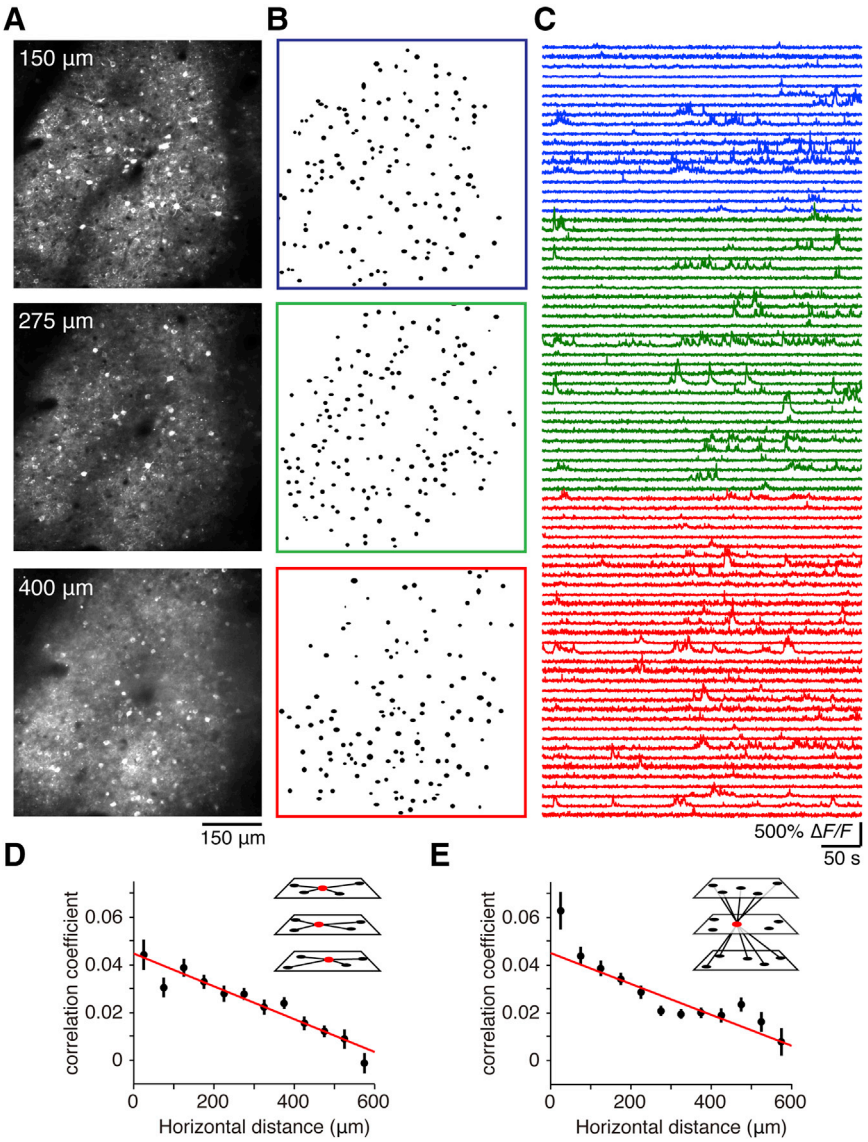

Figure 5. Three-Dimensional Imaging of Neuronal Population Activity in L2 and L3

(A) Representative two-photon images of GCaMP6f at a depth of 150 μm (top), 275 μm (middle), and 400 μm (bottom) from the cortical surface. These fields have the same horizontal location.

(B) ROI for activity analysis at each depth.

(C) Δ*F*/*F* traces of all active neurons over 400 s. Blue, green, and red indicate the traces of neurons at a depth of 150 μm, 275 μm, and 400 μm, respectively.

(D) Relation between pairwise correlation coefficient and horizontal cellular distance for 1,120 pairs of active neurons located at the same depth (from the same color traces shown in C). Red line indicates the linear regression line. Pairs were grouped every 50 μm. The error bars denote SEM.

(E) Relation between pairwise correlation coefficient and horizontal cellular distance for 1,508 pairs of active neurons located at different depths (from blue and green traces and from green and red traces; shown in C).

The importance of research on marmosets to biomedical and neuroscience research has recently increased (Kishi et al., 2014). The germline transmittable transgenic marmoset technique (Sasaki et al., 2009) offers an opportunity to generate genetically engineered primate models for studies on normal neuronal function and neurological disorders. Marmosets live as families in the wild and can be housed as a group in laboratory cages, which offers the opportunity to investigate social behaviors and their underlying neural mechanisms. There are already precedents of such studies in which vocal and cognitive behaviors were examined under free-moving conditions (Miller et al., 2010; Takemoto et al., 2011; Yamazaki et al., 2011). Of critical importance for two-photon imaging studies, it was recently shown that head-restrained marmosets can perform simple tasks (Mitchell et al., 2014; Remington et al., 2012). Combined with our technique, GECIs with red fluorescence at an excitation wavelength >1,000 nm may eventually allow the observation of neuronal activity in the deep layers (i.e., >1.2 mm depth) of the marmoset cortex (Akerboom et al., 2013; Inoue et al., 2015; Ohkura et al., 2012).

In conclusion, our technique removes a major obstacle to studying the non-human primate cortex using calcium imaging. In future studies, the technique, combined with various cognitive tasks, should shed light on the organization and plasticity of the primate cerebral cortex.

EXPERIMENTAL PROCEDURES

Animals

The Institutional Animal Care and Use Committee of National Institutes of Natural Sciences, Japan, approved all experiments. Five laboratory-bred adult common marmosets (*Callithrix jacchus*; one male and four females) were used. The marmosets were 46–52 months old (weight: 310–433 g). All marmosets were in a 12:12 hr light-dark cycle and were not used for other experiments prior to the present study.

Vector Production

The plasmid AAV:Thy1S-tTA was constructed by subcloning the DNA fragments containing the truncated Thy1S promoter (2.9 kb) and tTA into pAAV-MCS (Agilent Technologies). Thy1S promoter contains the 5′ region of the original Thy1 promoter and lacks its exon 4 and 3′ UTR (Ako et al., 2011). We further truncated its 5′ end for use in the AAV vector. The original Thy1 promoter (6.5 kb) may drive expression in GABAergic neurons (Lee et al., 2006). The plasmid AAV:SynI-rtTA (Watakabe et al., 2014) contains rtTV16 TET-On activator connected to the human Synapsin I promoter. The plasmid AAV:TRE3-GCaMP6f was constructed by subcloning TRE3 from TRE3-ZsGreen1 (Clontech), GCaMP6f from pGP-CMV-GCaMP6 (Addgene plasmid 40755), and WPRE from pAAV-Ef1a-DIO hChR2 (E123T/T159C)-EYFP (Addgene plasmid 35509). Thy1S-tTA and TRE3-GCaMP6f of the AAV vectors have capsids of serotype 1. SynI-rtTA of the AAV vector has capsids of serotype 9. They were produced in HEK293 cells using a helper-virus-free system, purified twice by

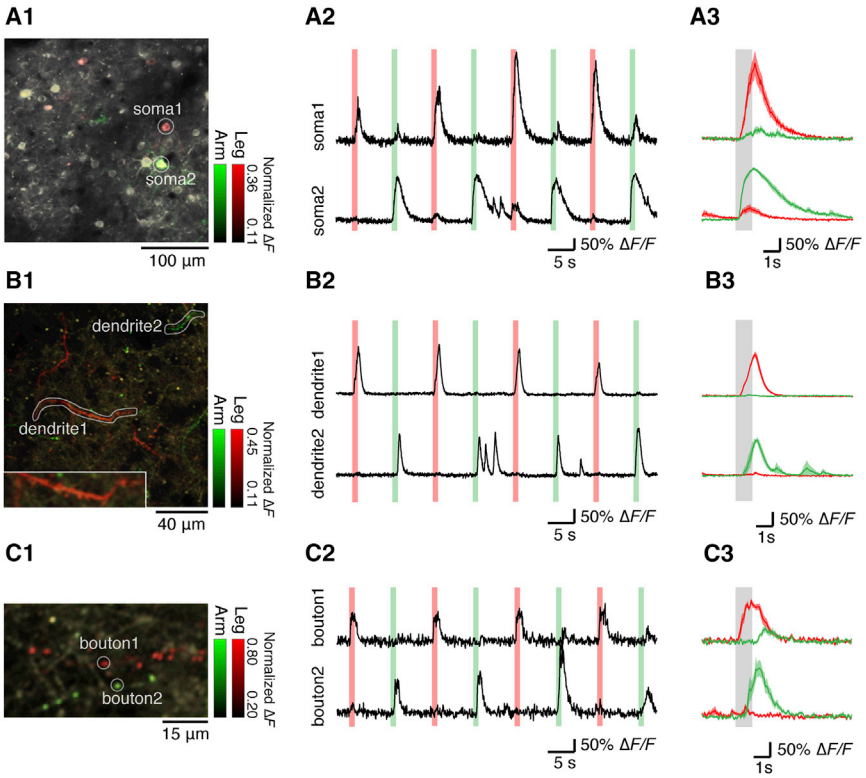

Figure 6. Selective Sensory Responses to Tactile Stimulation from Neuronal Somata, Dendrites, and Axonal Boutons

(A) Sensory responses to tactile stimulation from soma regions in the right somatosensory cortex. The depth of the image is 210 μm. (A1) Representative two-photon images on which colored stimulus selectivity (green, left arm; red, left leg) is overlaid are shown. In each stimulation condition, the stimulus selectivity for each pixel was defined by dividing Δ*F* during the stimulation averaged across all trials by the maximum value of the averaged Δ*F* of all pixels in each field in both conditions. (A2) Representative Δ*F*/*F* traces from two neurons indicated in A1 (soma 1 and soma 2) are shown. The green and red lines indicate the timing of tactile stimulation to the left arm and the left leg, respectively. (A3) Averaged Δ*F*/*F* traces from soma 1 and soma 2 aligned to the left arm (green) and the left leg (red) stimulation are shown. The responses to nine stimuli to each body part were averaged. The gray band indicates the timing of the left arm and the left leg stimulation.

(B) Sensory responses to tactile stimulation from dendrites in the right somatosensory cortex. The depth of the image is 15 μm. (B1) Representative two-photon images on which colored stimulus selectivity (green, left arm; red, left leg) is overlaid are shown. (B2) Representative Δ*F*/*F* traces from two dendrites indicated in (B1) (dendrite 1 and dendrite 2) are shown. (B3) Averaged Δ*F*/*F* traces from dendrite 1 and dendrite 2 aligned to the left arm (green) and the left leg (red) stimulation are shown.

(C) Sensory responses to tactile stimulation from axonal boutons in the right somatosensory cortex. The depth of the image is 20 μm. (C1) Representative two-photon images on which colored stimulus selectivity (green, left arm; red, left leg) is overlaid are shown. (C2) Representative Δ*F*/*F* traces from two axonal boutons indicated in C1 (bouton 1 and bouton 2) are shown. (C3) Averaged Δ*F*/*F* traces from bouton 1 and bouton 2 aligned to the left arm (green) and the left leg (red) stimulation are shown.

See also Movie S1.

$CsCl_2$ density gradient centrifugation, and titrated by qPCR, as described previously (Konishi et al., 2008). The final preparations were dialyzed against PBS and diluted as described below. To prevent adhesion of the AAV vector to glass micropipettes, 0.001% Pluronic-F68 (Sigma-Aldrich) was included in the vector solution. rAAV2/1-SynI-GCaMP6f was obtained from the University of Pennsylvania Gene Therapy Program Vector Core.

Vector Injection

All surgical procedures and AAV vector injections were performed under aseptic conditions. At first, ketamine (20 mg kg^{-1}) as an anesthetic agent, medetomidine (60 μg kg^{-1}) as a sedative and analgesic, ampicillin (40 mg kg^{-1}) as an antibiotic, and carprofen (5 mg kg^{-1}) as an anti-inflammatory agent were administered intramuscularly. Marmosets were then placed in a stereotaxic apparatus with anesthesia maintained using inhaled isoflurane (1.5%–2.5% in oxygen). Pulse oxygen (SpO_2), heart rate, and rectal temperature were continuously monitored to judge the marmoset's condition.

A 4-mm-diameter circular craniotomy was made over the right parietal or somatosensory cortex (Hardman and Ashwell, 2012; Yuasa et al., 2010), and the underlying dura mater was removed. Vector injections were performed using a pulled glass pipette (70 μm outer diameter) attached to a nanoliter 2000 injector connected to Micro4 controller (World Precision instrument). The viral preparations were adjusted to the final concentration of 0.04–1 × 10^{12} vg ml^{-1} for rAAV2/1-Thy1S-tTA and 1–5 × 10^{12} vg ml^{-1} for rAAV2/1-TRE3-GCaMP6f (n = 2 marmosets), 5 × 10^{12} vg ml^{-1} for rAAV2/9-SynI-rtTA and 1 × 10^{12} vg ml^{-1} for rAAV2/1-TRE3-GCaMP6f (n = 1 marmoset), and 0.2–1 × 10^{12} vg ml^{-1} for rAAV2/1-SynI-GCaMP6f (n = 2 marmosets). The mixture of these AAVs was injected at 0.1 μl min^{-1} for 5 min at a depth of 0.5 mm from the cortical surface. A window, which was composed of a 5.5-mm circular glass coverslip (approximately 100 μm thickness; Matsunami Glass) cemented to four sheets of 3-mm circular glass coverslips (approximately 300 μm thickness; Matsunami Glass) with UV-curing optical adhesives (NOR-61; Norland Products), was pressed onto the brain surface, and the edge was sealed with dental cement (Fuji Lute BC; GC) and dental adhesive resin cement (Super bond; Sun Medical). Finally, a head plate (CFR-1; Narishige) was attached to the skull using quick self-curing acrylic resin (UNIFAST II; GC) and four small screws. After that, marmosets were single caged to avoid damaging the head plate and the glass window.

Administration of Dox

For TET-Off and TET-On systems, oral administration of Dox was initiated 10 days, 58 days, and 104 days after the virus injection (marmoset A for TET-Off); 13 days after the virus injection (marmoset B for TET-Off); and 25 days after the virus injection (another marmoset for TET-On). Dox was administered orally in drinking water (0.1–0.2 mg ml^{-1} in a 1.25%–2.5% sucrose solution) for 1–17 days (Figure S3).

Two-Photon Imaging

The anesthetized marmoset was head restrained to a custom-made marmoset chair (O'Hara & Co.) with head holders (SR-10R-HT; Narishige) under a multiphoton laser scanning microscope equipped with a gantry frame system (FVMPE-RS; Olympus). Inhaled isoflurane was 0.5%–1% in oxygen during imaging of spontaneous neural activity, 0.25%–0.5% in oxygen during imaging of sensory-evoked neural activity, and 1%–1.5% in oxygen during chronic imaging. During imaging of sensory-evoked neural activity, medetomidine (20 μg kg^{-1})

as a sedative and analgesic was also administered intramuscularly, SpO_2 and heart rate were continuously monitored to check the marmoset's condition, and the marmoset's body was warmed by a heating pad.

Two-photon imaging was conducted with FVMPE-RS equipped with a broadly tunable ultrafast laser (InSight DeepSee; Spectra Physics) at a wavelength of 940 nm. In each imaging session, the plane of the imaging window was adjusted to be nearly perpendicular to the optical axis (~5–10 degrees) by tilting the Goniometer Rotation Stage (Olympus) attached to the marmoset chair. During imaging of spontaneous neural activity and sensory-evoked neural activity, fluorescence emissions were divided using a 570-nm dichroic mirror and the short-wavelength side of the emissions was directly collected with a GaAsP photomultiplier tube (Hamamatsu Photonics). During chronic imaging, fluorescence emissions were collected without the dichroic mirror and the bright-field image of blood vessels on the brain's surface and the intrinsic fluorescence of blood vessels in the brain at a wavelength of 940 nm were used to orient to the same imaging location.

For all experiments, a 10× objective (XLPLN10XSVMP; numerical aperture of 0.6; working distance of 8 mm; Olympus) was used. Because of the size limit of the scanning mirrors, the back aperture of the objective was underfilled with a laser beam with a diameter of 15.1 mm. The practical numerical aperture of the objective was calculated as 0.42. The laser power to image the marmoset cortical tissue was typically 38–69 mW after the objective (max 120 mW at 400 μm depth from the cortical surface). For imaging of neural activity, images were acquired at a frame rate of 30 Hz with a resonant scanner and a galvano scanner in somata (512 × 512 pixels, with a spatial resolution of 0.828 × 0.828 μm pixel^{-1} or 1.241 × 1.241 μm pixel^{-1}) and dendrites (512 × 512 pixels, with a spatial resolution of 0.310 × 0.310 μm pixel^{-1}) and at a frame rate of 16.6 Hz with a galvano scanner in axons (124 × 44 pixels, with a spatial resolution of 0.653 × 0.653 μm pixel^{-1}). For chronic imaging, images were acquired at a frame rate of 0.25 Hz with two galvano scanners (1,024 × 1,024 pixels, with a spatial resolution of 1.24 × 1.24 μm pixel^{-1} or 0.620 × 0.620 μm pixel^{-1}). To minimize the effect of spontaneous changes in the baseline fluorescence intensity that was compared across imaging days, five consecutive frames were averaged.

To evaluate the validity of the usage of the relatively thick (approximately 1.3 mm) glass coverslips for the imaging window, fluorescent yellow-green beads with a diameter of 2 μm (Fluoresbrite YG Plain Microspheres; Polysciences) were imaged with and without the glass coverslips. The beads were diluted to 100 times by 2% agarose gel in water (agarose L; Nippon Gene), and the glass coverslip was placed on the agarose surface. The beads were <50 μm from the bottom of the glass window. The optical resolution of the two-photon imaging through the glass window was slightly lower than that without the glass window (mean ± SD lateral resolution: 1.49 ± 0.042 μm versus 1.99 ± 0.21 μm; axial resolution: 7.66 ± 0.2 μm versus 8.53 ± 0.66 μm; n = 5 beads) but was comparable to that obtained by two-photon imaging using a GRIN lens that could detect the activity not only in the cell body but also in the dendrite (Lecoq et al., 2014). Thus, the usage of the glass window developed in the present study was valid for two-photon imaging of the marmoset neocortex.

Sensory Stimulation

The left arm and the left leg were alternatively stimulated for 1 s by a flat coreless vibration motor (FM34F; Tokyo Parts Industrial) at an interval of 7.5 s. A program written with LabVIEW (2013SP1; National Instruments) was used to regulate the timing of the sensory stimulation.

Image Processing

Analyses of images were performed using ImageJ software (1.49d; NIH) and MATLAB software (R2013b; MathWorks). Image sequences were corrected for focal plane displacements with the ImageJ plug-in, TurboReg (Thévenaz et al., 1998). ROIs were determined manually to surround the putative neuronal soma. The $\Delta F/F$ in each ROI was calculated, and the baseline fluorescence intensity was set to be the eighth percentile value of the fluorescence distribution of each consecutive recording. To calculate the half-decay time of calcium transients in Figures 2F and 2G, calcium transients with a peak of greater than four SDs of $\Delta F/F$ traces that had no other peak from 0.5 s before to 1 s after the identified peak were selected and averaged for each ROI.

Immunohistochemistry

Immunohistochemistry was performed as previously described (Watakabe et al., 2015). Briefly, the marmoset was deeply anesthetized by an intraperitoneal injection of sodium pentobarbital and perfused transcardially with 0.9% NaCl, followed by fixation with 4% paraformaldehyde in 0.1 M PBS (pH 7.4). The cryoprotected marmoset brain was sliced with a thickness of 40–50 μm. For immunostaining of the marmoset that received the rAAV2/1-SynI-GCaMP6f injection, the antibody to GFP (rabbit IgG; 1:20,000; Tamamaki et al., 2000) was used as the primary antibody. For immunostaining of the marmoset that received the AAV-TET-Off vectors injection, the native fluorescence of GCaMP6f was counterstained with anti-NeuN (mouse IgG; 1:2,000; cat. no. MAB377; Millipore) or with anti-parvalbumin antibody (rabbit IgG; 1:2,000; Swant), followed by visualization by staining with Cy3-conjugated anti-mouse or anti-rabbit secondary antibodies (1:1,000; Jackson ImmunoResearch). The fluorescent images were captured by an Olympus DP71 digital camera attached to a BX51 microscope (Olympus). The confocal images were taken using the Nikon confocal laser microscope system A1 (Nikon). Maximum intensity projection images for the confocal data were created by NIS-Elements imaging software (Nikon). All images were processed by Adobe Photoshop CS5 to achieve the proper contrast for presentation.

SUPPLEMENTAL INFORMATION

Supplemental Information includes five figures and one movie and can be found with this article online at http://dx.doi.org/10.1016/j.celrep.2015.10.050.

AUTHOR CONTRIBUTIONS

O.S., Y.M., A.W., S.-I.T., M.M., and T.Y. designed the experiments. O.S., Y.M., A.W., M.O., and S.-I.T. conducted the experiments. A.W., M.T., H.M., K.O., and H.K. designed and prepared an AAV vector system. A.W. and S.-I.T. analyzed data. O.S., Y.M., A.W., S.-I.T., M.M., and T.Y. wrote the paper, with comments from all authors.

ACKNOWLEDGMENTS

We thank V. Jayaraman, R. Kerr, D. Kim, L. Looger, and K. Svoboda of the GENIE Project Janelia Farm Research Campus (HHMI) for providing rAAV2/1-SynI-GCaMP6f and pGP-CMV-GCaMP6 and K. Deisseroth of Stanford University for providing pAAV-Ef1a-DIO hChR2 (E123T/T159C)-EYFP. We thank R. Hira and Y. Isomura for the development of the custom-made marmoset chair. We thank E. Sasaki for helpful advice for handling marmosets as well as for providing two of our experimental animals. We thank S. Ohsawa and J. Wang for help with histology and Y. Takeda, R. Hirakawa, Y. Takahashi, E. Imoto, E. Iwase, and K. Kotani for animal handling. Confocal images were acquired at Spectrography and Bioimaging Facility, NIBB Core Research Facilities. The research was supported by Scientific Research on Innovative Areas to T.Y. (22123009), a grant from JSPS to A.W. (KAKENHI 40290910 and 22500300), Grants-in-Aid for Scientific Research A to T.Y. (20240030), a JSPS Research Fellowship for Young Scientists to S.-I.T., the Strategic Research Program for Brain Sciences to M.M. and T.Y., and the program for Brain Mapping by Integrated Neurotechnologies for Disease Studies (Brain/MINDS) from MEXT and AMED, Japan, to M.M. and T.Y.

Received: June 18, 2015
Revised: August 28, 2015
Accepted: October 15, 2015
Published: November 19, 2015

REFERENCES

Akerboom, J., Carreras Calderón, N., Tian, L., Wabnig, S., Prigge, M., Tolö, J., Gordus, A., Orger, M.B., Severi, K.E., Macklin, J.J., et al. (2013). Genetically encoded calcium indicators for multi-color neural activity imaging and combination with optogenetics. Front. Mol. Neurosci. *6*, 2.

Ako, R., Wakimoto, M., Ebisu, H., Tanno, K., Hira, R., Kasai, H., Matsuzaki, M., and Kawasaki, H. (2011). Simultaneous visualization of multiple neuronal properties with single-cell resolution in the living rodent brain. Mol. Cell. Neurosci. *48*, 246–257.

Andermann, M.L., Kerlin, A.M., Roumis, D.K., Glickfeld, L.L., and Reid, R.C. (2011). Functional specialization of mouse higher visual cortical areas. Neuron *72*, 1025–1039.

Chen, J.L., Carta, S., Soldado-Magraner, J., Schneider, B.L., and Helmchen, F. (2013a). Behaviour-dependent recruitment of long-range projection neurons in somatosensory cortex. Nature *499*, 336–340.

Chen, T.-W., Wardill, T.J., Sun, Y., Pulver, S.R., Renninger, S.L., Baohan, A., Schreiter, E.R., Kerr, R.A., Orger, M.B., Jayaraman, V., et al. (2013b). Ultrasensitive fluorescent proteins for imaging neuronal activity. Nature *499*, 295–300.

Dancause, N., Barbay, S., Frost, S.B., Plautz, E.J., Chen, D., Zoubina, E.V., Stowe, A.M., and Nudo, R.J. (2005). Extensive cortical rewiring after brain injury. J. Neurosci. *25*, 10167–10179.

Diester, I., Kaufman, M.T., Mogri, M., Pashaie, R., Goo, W., Yizhar, O., Ramakrishnan, C., Deisseroth, K., and Shenoy, K.V. (2011). An optogenetic toolbox designed for primates. Nat. Neurosci. *14*, 387–397.

Eichhoff, G., Busche, M.A., and Garaschuk, O. (2008). In vivo calcium imaging of the aging and diseased brain. Eur. J. Nucl. Med. Mol. Imaging *35* (*Suppl 1*), S99–S106.

Flor, H., Elbert, T., Knecht, S., Wienbruch, C., Pantev, C., Birbaumer, N., Larbig, W., and Taub, E. (1995). Phantom-limb pain as a perceptual correlate of cortical reorganization following arm amputation. Nature *375*, 482–484.

Gerits, A., and Vanduffel, W. (2013). Optogenetics in primates: a shining future? Trends Genet. *29*, 403–411.

Glickfeld, L.L., Andermann, M.L., Bonin, V., and Reid, R.C. (2013). Cortico-cortical projections in mouse visual cortex are functionally target specific. Nat. Neurosci. *16*, 219–226.

Hardman, C.D., and Ashwell, K.W.S. (2012). Stereotaxic and Chemoarchitectural Atlas of the Brain of the Common Marmoset (Callithrix jacchus) (Boca Raton, FL: CRC Press).

Harvey, C.D., Coen, P., and Tank, D.W. (2012). Choice-specific sequences in parietal cortex during a virtual-navigation decision task. Nature *484*, 62–68.

Heider, B., Nathanson, J.L., Isacoff, E.Y., Callaway, E.M., and Siegel, R.M. (2010). Two-photon imaging of calcium in virally transfected striate cortical neurons of behaving monkey. PLoS ONE *5*, e13829.

Hioki, H., Kuramoto, E., Konno, M., Kameda, H., Takahashi, Y., Nakano, T., Nakamura, K.C., and Kaneko, T. (2009). High-level transgene expression in neurons by lentivirus with Tet-Off system. Neurosci. Res. *63*, 149–154.

Hofer, S.B., Ko, H., Pichler, B., Vogelstein, J., Ros, H., Zeng, H., Lein, E., Lesica, N.A., and Mrsic-Flogel, T.D. (2011). Differential connectivity and response dynamics of excitatory and inhibitory neurons in visual cortex. Nat. Neurosci. *14*, 1045–1052.

Honavar, M., and Lantos, P.L. (1987). Ultrastructural changes in the frontal cortex and hippocampus in the ageing marmoset. Mech. Ageing Dev. *41*, 161–175.

Huber, D., Gutnisky, D.A., Peron, S., O'Connor, D.H., Wiegert, J.S., Tian, L., Oertner, T.G., Looger, L.L., and Svoboda, K. (2012). Multiple dynamic representations in the motor cortex during sensorimotor learning. Nature *484*, 473–478.

Ikezoe, K., Mori, Y., Kitamura, K., Tamura, H., and Fujita, I. (2013). Relationship between the local structure of orientation map and the strength of orientation tuning of neurons in monkey V1: a 2-photon calcium imaging study. J. Neurosci. *33*, 16818–16827.

Inoue, M., Takeuchi, A., Horigane, S., Ohkura, M., Gengyo-Ando, K., Fujii, H., Kamijo, S., Takemoto-Kimura, S., Kano, M., Nakai, J., et al. (2015). Rational design of a high-affinity, fast, red calcium indicator R-CaMP2. Nat. Methods *12*, 64–70.

Kawakami, R., Sawada, K., Sato, A., Hibi, T., Kozawa, Y., Sato, S., Yokoyama, H., and Nemoto, T. (2013). Visualizing hippocampal neurons with in vivo two-photon microscopy using a 1030 nm picosecond pulse laser. Sci. Rep. *3*, 1014.

Khodagholy, D., Gelinas, J.N., Thesen, T., Doyle, W., Devinsky, O., Malliaras, G.G., and Buzsáki, G. (2015). NeuroGrid: recording action potentials from the surface of the brain. Nat. Neurosci. *18*, 310–315.

Kinoshita, M., Matsui, R., Kato, S., Hasegawa, T., Kasahara, H., Isa, K., Watakabe, A., Yamamori, T., Nishimura, Y., Alstermark, B., et al. (2012). Genetic dissection of the circuit for hand dexterity in primates. Nature *487*, 235–238.

Kishi, N., Sato, K., Sasaki, E., and Okano, H. (2014). Common marmoset as a new model animal for neuroscience research and genome editing technology. Dev. Growth Differ. *56*, 53–62.

Konishi, M., Kawamoto, K., Izumikawa, M., Kuriyama, H., and Yamashita, T. (2008). Gene transfer into guinea pig cochlea using adeno-associated virus vectors. J. Gene Med. *10*, 610–618.

Krubitzer, L.A., and Kaas, J.H. (1990). The organization and connections of somatosensory cortex in marmosets. J. Neurosci. *10*, 952–974.

Lecoq, J., Savall, J., Vučinić, D., Grewe, B.F., Kim, H., Li, J.Z., Kitch, L.J., and Schnitzer, M.J. (2014). Visualizing mammalian brain area interactions by dual-axis two-photon calcium imaging. Nat. Neurosci. *17*, 1825–1829.

Lee, W.C.A., Huang, H., Feng, G., Sanes, J.R., Brown, E.N., So, P.T., and Nedivi, E. (2006). Dynamic remodeling of dendritic arbors in GABAergic interneurons of adult visual cortex. PLoS Biol. *4*, e29.

Lewandoski, M. (2001). Conditional control of gene expression in the mouse. Nat. Rev. Genet. *2*, 743–755.

Liu, X., Ramirez, S., Pang, P.T., Puryear, C.B., Govindarajan, A., Deisseroth, K., and Tonegawa, S. (2012). Optogenetic stimulation of a hippocampal engram activates fear memory recall. Nature *484*, 381–385.

Masamizu, Y., Okada, T., Kawasaki, K., Ishibashi, H., Yuasa, S., Takeda, S., Hasegawa, I., and Nakahara, K. (2011). Local and retrograde gene transfer into primate neuronal pathways via adeno-associated virus serotype 8 and 9. Neuroscience *193*, 249–258.

Masamizu, Y., Tanaka, Y.R., Tanaka, Y.H., Hira, R., Ohkubo, F., Kitamura, K., Isomura, Y., Okada, T., and Matsuzaki, M. (2014). Two distinct layer-specific dynamics of cortical ensembles during learning of a motor task. Nat. Neurosci. *17*, 987–994.

Matsui, T., and Ohki, K. (2013). Target dependence of orientation and direction selectivity of corticocortical projection neurons in the mouse V1. Front. Neural Circuits *7*, 143.

Merzenich, M.M., Nelson, R.J., Stryker, M.P., Cynader, M.S., Schoppmann, A., and Zook, J.M. (1984). Somatosensory cortical map changes following digit amputation in adult monkeys. J. Comp. Neurol. *224*, 591–605.

Miller, C.T., Mandel, K., and Wang, X. (2010). The communicative content of the common marmoset phee call during antiphonal calling. Am. J. Primatol. *72*, 974–980.

Mitchell, J.F., Reynolds, J.H., and Miller, C.T. (2014). Active vision in marmosets: a model system for visual neuroscience. J. Neurosci. *34*, 1183–1194.

Mitz, A.R., Godschalk, M., and Wise, S.P. (1991). Learning-dependent neuronal activity in the premotor cortex: activity during the acquisition of conditional motor associations. J. Neurosci. *11*, 1855–1872.

Mochizuki, Y., Park, M.K., Mori, T., and Kawashima, S. (1995). The difference in autofluorescence features of lipofuscin between brain and adrenal. Zoolog. Sci. *12*, 283–288.

Nauhaus, I., Nielsen, K.J., Disney, A.A., and Callaway, E.M. (2012). Orthogonal micro-organization of orientation and spatial frequency in primate primary visual cortex. Nat. Neurosci. *15*, 1683–1690.

O'Connor, D.H., Peron, S.P., Huber, D., and Svoboda, K. (2010). Neural activity in barrel cortex underlying vibrissa-based object localization in mice. Neuron *67*, 1048–1061.

Ohkura, M., Sasaki, T., Kobayashi, C., Ikegaya, Y., and Nakai, J. (2012). An improved genetically encoded red fluorescent Ca^{2+} indicator for detecting optically evoked action potentials. PLoS ONE *7*, e39933.

Peters, A.J., Chen, S.X., and Komiyama, T. (2014). Emergence of reproducible spatiotemporal activity during motor learning. Nature *510*, 263–267.

Petreanu, L., Gutnisky, D.A., Huber, D., Xu, N.L., O'Connor, D.H., Tian, L., Looger, L., and Svoboda, K. (2012). Activity in motor-sensory projections reveals distributed coding in somatosensation. Nature *489*, 299–303.

Remington, E.D., Osmanski, M.S., and Wang, X. (2012). An operant conditioning method for studying auditory behaviors in marmoset monkeys. PLoS ONE *7*, e47895.

Roberts, A.C., Tomic, D.L., Parkinson, C.H., Roeling, T.A., Cutter, D.J., Robbins, T.W., and Everitt, B.J. (2007). Forebrain connectivity of the prefrontal cortex in the marmoset monkey (Callithrix jacchus): an anterograde and retrograde tract-tracing study. J. Comp. Neurol. *502*, 86–112.

Sasaki, E., Suemizu, H., Shimada, A., Hanazawa, K., Oiwa, R., Kamioka, M., Tomioka, I., Sotomaru, Y., Hirakawa, R., Eto, T., et al. (2009). Generation of transgenic non-human primates with germline transmission. Nature *459*, 523–527.

Sooksawate, T., Isa, K., Matsui, R., Kato, S., Kinoshita, M., Kobayashi, K., Watanabe, D., Kobayashi, K., and Isa, T. (2013). Viral vector-mediated selective and reversible blockade of the pathway for visual orienting in mice. Front. Neural Circuits *7*, 162.

Stettler, D.D., Yamahachi, H., Li, W., Denk, W., and Gilbert, C.D. (2006). Axons and synaptic boutons are highly dynamic in adult visual cortex. Neuron *49*, 877–887.

Takemoto, A., Izumi, A., Miwa, M., and Nakamura, K. (2011). Development of a compact and general-purpose experimental apparatus with a touch-sensitive screen for use in evaluating cognitive functions in common marmosets. J. Neurosci. Methods *199*, 82–86.

Tamamaki, N., Nakamura, K., Furuta, T., Asamoto, K., and Kaneko, T. (2000). Neurons in Golgi-stain-like images revealed by GFP-adenovirus infection in vivo. Neurosci. Res. *38*, 231–236.

Thévenaz, P., Ruttimann, U.E., and Unser, M. (1998). A pyramid approach to subpixel registration based on intensity. IEEE Trans. Image Process. *7*, 27–41.

Tian, L., Hires, S.A., Mao, T., Huber, D., Chiappe, M.E., Chalasani, S.H., Petreanu, L., Akerboom, J., McKinney, S.A., Schreiter, E.R., et al. (2009). Imaging neural activity in worms, flies and mice with improved GCaMP calcium indicators. Nat. Methods *6*, 875–881.

Watakabe, A., Kato, S., Kobayashi, K., Takaji, M., Nakagami, Y., Sadakane, O., Ohtsuka, M., Hioki, H., Kaneko, T., Okuno, H., et al. (2012). Visualization of cortical projection neurons with retrograde TET-off lentiviral vector. PLoS ONE *7*, e46157.

Watakabe, A., Takaji, M., Kato, S., Kobayashi, K., Mizukami, H., Ozawa, K., Ohsawa, S., Matsui, R., Watanabe, D., and Yamamori, T. (2014). Simultaneous visualization of extrinsic and intrinsic axon collaterals in Golgi-like detail for mouse corticothalamic and corticocortical cells: a double viral infection method. Front. Neural Circuits *8*, 110.

Watakabe, A., Ohtsuka, M., Kinoshita, M., Takaji, M., Isa, K., Mizukami, H., Ozawa, K., Isa, T., and Yamamori, T. (2015). Comparative analyses of adeno-associated viral vector serotypes 1, 2, 5, 8 and 9 in marmoset, mouse and macaque cerebral cortex. Neurosci. Res. *93*, 144–157.

Xu, N.L., Harnett, M.T., Williams, S.R., Huber, D., O'Connor, D.H., Svoboda, K., and Magee, J.C. (2012). Nonlinear dendritic integration of sensory and motor input during an active sensing task. Nature *492*, 247–251.

Yamazaki, Y., Echigo, C., Saiki, M., Inada, M., Watanabe, S., and Iriki, A. (2011). Tool-use learning by common marmosets (Callithrix jacchus). Exp. Brain Res. *213*, 63–71.

Yuasa, S., Nakamura, K., and Kohsaka, S. (2010). Stereotaxic Atlas of the Marmoset Brain with Immunohistochemical Architecture and MR Images (Tokyo: Igaku Shoin).